

Convergence analysis for image interpolation in terms of the cSSIM

Francesco Marchetti ^{*1} and Gabriele Santin ⁺²

¹University of Padova, Padova, Italy

²Bruno Kessler Foundation, Trento, Italy

August 10, 2021

Abstract

Assessing the similarity of two images is a complex task that has attracted significant efforts in the image processing community. The widely used Structural Similarity Index Measure (SSIM) addresses this problem by quantifying a perceptual structural similarity.

In this paper we consider a recently introduced continuous SSIM (cSSIM), which allows one to analyze sequences of images of increasingly fine resolutions. We prove that this index includes the classical SSIM as a special case, and we provide a precise connection between image similarity measured by the cSSIM and by the L_2 norm.

Using this connection, we derive bounds on the cSSIM by means of bounds on the L_2 error, and we even prove that the two error measures are equivalent in certain circumstances. We exploit these results to obtain precise rates of convergence with respect to the cSSIM for several concrete image interpolation methods, and we further validate these findings by many numerical experiments.

This newly established connection paves the way to obtain novel insights into the features and limitations of the SSIM.

^{*}francesco.marchetti@math.unipd.it, orcid.org/0000-0003-1087-7589

[†]gsantin@fbk.eu, orcid.org/0000-0001-6959-1070

1 Introduction

Image interpolation is a widely-investigated topic in image processing and concerns various applications, such as super-resolution, image resizing, image rotation and registration. Therefore, many different interpolation techniques have been developed in the last decades. Nearest-neighbor, bilinear and bicubic interpolation are classical fast polynomial-based approaches [12, 18, 21], which however present limitations especially in presence of edges [20]. Thus, in order to treat the resulting artifacts, adaptive techniques have been proposed [1, 13, 14].

In certain applications, an image needs to be reconstructed by interpolating at non-gridded data sites. In this case, unless it is possible to exploit some particular properties concerning the distribution of the samples [7], a kernel-based approach guarantees the flexibility required when dealing with scattered data [8, 9].

Furthermore, various deep learning strategies based upon Convolutional Neural Networks (CNNs) have been designed in the last years and turned out to be accurate and efficient tools in many tasks [6, 11, 25, 26].

Evaluating the adherence of the final reconstruction to the original image is itself a challenging task, and classical error metrics have been found to be unsuitable for this task in many cases. The Structural Similarity Index Measure (SSIM) [22] is a widely

considered metric that aims at quantifying the *visually perceived* quality of the reconstruction. In the last years its mathematical properties have been thoroughly investigated, and different result have been derived [4, 5]. Moreover, modifications of the SSIM has been proposed, as in, e.g., [19, 17]. In particular, the continuous SSIM (cSSIM) has been introduced in [15] as the extension of the *discrete* SSIM to the continuous framework. There, the convergence rate of a kernel-based interpolant in terms of the cSSIM has been analysed in terms of the supremum norm.

In this work, we consider the cSSIM and start by proving that it is indeed a limit version of the SSIM as the resolution of the image gets larger. Then, in Section 3, we analyse the cSSIM in terms of the L_2 norm. Indeed, we provide both lower and upper bounds and we show that, under certain assumptions, the dissimilarity index ($1 - \text{cSSIM}$) is equivalent to the L_2 norm.

Such theoretical findings are therefore exploited in Section 4 to formulate accurate convergence rate estimates in terms of the cSSIM for bilinear, Hermite bicubic and kernel-based interpolation, which are confirmed by the numerical tests carried out in Section 5. Then, in Section 6, we perform some concrete image interpolation experiments, showing how the limitations in regularity affect the theoretically achieved convergence rates. The discussion of the obtained results, as well as some concluding remarks, are offered in Section 7.

2 The Structural Similarity Index and its continuous counterpart

We start by recalling the definitions of SSIM and cSSIM. Letting $F, G \in \mathbb{R}_{\geq 0}^{p \times q}$, $p, q \in \mathbb{N}$, be positive-valued matrices representing two single-channel images, the SSIM is defined as (see [22])

$$\text{SSIM}(F, G) := \frac{2\mu_F\mu_G + c_1}{\mu_F^2 + \mu_G^2 + c_1} \cdot \frac{2\sigma_{F,G} + c_2}{\sigma_F^2 + \sigma_G^2 + c_2}, \quad (1)$$

where μ_F, μ_G are the sample mean of F and G , whilst σ_F^2, σ_G^2 and $\sigma_{F,G}$ are the sample variances and covariance. The constants $c_1, c_2 > 0$ are stabilizing factors

that avoid division by zero, and can be tuned by the user.

Differently with respect to the classic SSIM, the definition of the cSSIM is natively not restricted to matrices. Indeed, we consider a bounded set $\Omega \subset \mathbb{R}^d$ and a probability measure ν on Ω . Moreover, we denote as $L_2^+(\Omega, \nu)$ the set of functions $f \in L_2(\Omega, \nu)$ with $f \geq 0$ ν -almost everywhere (ν -a.e. in the following). For $f, g \in L_2^+(\Omega, \nu)$ we define

$$\mu_f := \int_{\Omega} f d\nu = \|f\|_{L_1}, \quad (2)$$

$$\sigma_{fg} := \int_{\Omega} (f - \mu_f)(g - \mu_g) d\nu = \langle f - \mu_f, g - \mu_g \rangle_{L_2}.$$

Then the cSSIM between f and g is defined in [15] as

$$\text{cSSIM}_{\nu}(f, g) := \frac{2\mu_f\mu_g + c_1}{\mu_f^2 + \mu_g^2 + c_1} \cdot \frac{2\sigma_{fg} + c_2}{\sigma_{ff} + \sigma_{gg} + c_2}, \quad (3)$$

with the constants $c_1, c_2 > 0$ playing the same role as in the discrete case.

In the following, unless otherwise stated, we assume w.l.o.g. that ν is the normalized Lebesgue measure of Ω , and we simply write cSSIM, $L_2(\Omega)$, $L_2^+(\Omega)$.

Observe that the cSSIM is defined in general dimension d , and it is thus not restricted to images. A similar extension would be possible in the discrete case by considering d -channel matrices, i.e., $F, G \in \mathbb{R}_{\geq 0}^{p \times q \times d}$, and extending (1) in the obvious way.

We start by considering the relation between the two indices and we consider for simplicity the two dimensional case, even if the extension to higher dimensions is straightforward. The following proposition proves that the classical SSIM can be obtained from the cSSIM when ν is a discrete counting measure. On the other hand, the SSIM is a discretization of the cSSIM: if the continuous functions f, g are discretized to images of increasing resolution, then the SSIM of the discretizations converge to the cSSIM of the original functions.

Proposition 1. *Let $\Omega = [a, b] \times [c, d] \subset \mathbb{R}^2$, $a < b$, $c < d$, and let $f, g \in L_2^+(\Omega)$ be bounded and continuous almost everywhere on Ω . Let $m, n \in \mathbb{N}$,*

$m = cn$ with $c \in \mathbb{Q}$, and let $p_0, \dots, p_m, q_0, \dots, q_n$ be such that $p_i := c + i(d - c)/m$, $q_i := a + i(b - a)/n$ and $p_{i+1} - p_i = q_{i+1} - q_i$ for $i = 0, \dots, \min\{m, n\}$. We define the sequences of matrices $\{F_n\}_{n \in \mathbb{N}}$, $\{G_n\}_{n \in \mathbb{N}}$ as

$$F_n(i, j) := f(p_i, q_j), \quad G_n(i, j) := g(p_i, q_j),$$

$1 \leq i \leq m - 1$, $1 \leq j \leq n - 1$, so that F_n and G_n are $(m - 1) \times (n - 1)$ matrices. Moreover, let ν_n be the normalized counting measure supported on the points $\{(p_i, q_j)\}_{1 \leq i \leq m-1, 1 \leq j \leq n-1}$.

Then, we have

1. $\text{cSSIM}_{\nu_n}(f, g) = \text{SSIM}(F_n, G_n)$.
2. $\lim_{n \rightarrow \infty} \text{SSIM}(F_n, G_n) = \text{cSSIM}(f, g)$.

Proof. The first point follows directly from the definition (3) of the cSSIM.

To prove the second point we can associate to F_n, G_n the piece-wise constant functions on Ω

$$\begin{aligned} f_n &:= \sum_{i,j=0}^{m,n} f(p_i, q_j) \chi_{[p_i, p_{i+1}[\times [q_j, q_{j+1}[}, \\ g_n &:= \sum_{i,j=0}^{m,n} g(p_i, q_j) \chi_{[p_i, p_{i+1}[\times [q_j, q_{j+1}[}, \end{aligned}$$

where χ is the indicator function. Then, in this view, the sample means μ_{F_n} and μ_{G_n} of F_n and G_n are equivalent to the normalized Riemann integrals of f_n and g_n . Since f, g are bounded and continuous almost everywhere, such integrals converge then to the normalized Lebesgue means μ_f and μ_g as n tends to infinity. \square

Remark 2. As resulting from Proposition 1, the cSSIM can be interpreted as the SSIM computed on two infinite-resolution images. Alternatively, SSIM is a good approximation of the cSSIM as the resolution gets large enough.

3 Bounding the cSSIM via the L_2 norm

We are now interested in linking the cSSIM to more classical error metrics.

As a first step, we consider the two multiplicative terms that define the cSSIM in (3) and express them in terms of L_1 and L_2 norms. The following lemma

is a simple adaptation of the argument in [5, Section A], i.e., we just rephrase the same computations using the L_1 and L_2 norm instead of the discrete 2-norm used in the cited paper.

Lemma 3. For $f, g \in L_2^+(\Omega)$ and $c_1, c_2 > 0$ define

$$M(f, g) := \frac{2\mu_f \mu_g + c_1}{\mu_f^2 + \mu_g^2 + c_1}, \quad S(f, g) := \frac{2\sigma_{fg} + c_2}{\sigma_{ff} + \sigma_{gg} + c_2}.$$

Then

$$1 - M(f, g) \leq \frac{\|f - g\|_{L_1}^2}{\mu_f^2 + \mu_g^2 + c_1} \quad (4)$$

$$1 - S(f, g) = \frac{\|(f - \mu_f) - (g - \mu_g)\|_{L_2}^2}{\sigma_{ff} + \sigma_{gg} + c_2}. \quad (5)$$

Proof. By direct computation we have

$$\begin{aligned} 1 - M(f, g) &= 1 - \frac{2\mu_f \mu_g + c_1}{\mu_f^2 + \mu_g^2 + c_1} \\ &= \frac{\mu_f^2 + \mu_g^2 + c_1 - 2\mu_f \mu_g - c_1}{\mu_f^2 + \mu_g^2 + c_1} \\ &= \frac{(\mu_f - \mu_g)^2}{\mu_f^2 + \mu_g^2 + c_1}. \end{aligned}$$

Moreover, the numerator in last term can be bounded via

$$\mu_f - \mu_g = \int_{\Omega} (f - g) dx \leq \int_{\Omega} |f - g| dx = \|f - g\|_{L_1},$$

and this proves (4).

Similarly, for S we obtain

$$\begin{aligned} 1 - S(f, g) &= 1 - \frac{2\sigma_{fg} + c_2}{\sigma_{ff} + \sigma_{gg} + c_2} \\ &= \frac{\sigma_{ff} + \sigma_{gg} + c_2 - 2\sigma_{fg} - c_2}{\sigma_{ff} + \sigma_{gg} + c_2} \\ &= \frac{\sigma_{ff} + \sigma_{gg} - 2\sigma_{fg}}{\sigma_{ff} + \sigma_{gg} + c_2}, \end{aligned}$$

and in this case we have

$$\begin{aligned}\sigma_{ff} + \sigma_{gg} - 2\sigma_{fg} &= \\ &= \left\| f - \mu_f \right\|_{L_2}^2 + \left\| g - \mu_g \right\|_{L_2}^2 - 2 \left\langle f - \mu_f, g - \mu_g \right\rangle_{L_2} \\ &= \left\| (f - \mu_f) - (g - \mu_g) \right\|_{L_2}^2,\end{aligned}$$

which proves (5). \square

Next, we prove a simple condition of M and S .

Lemma 4. *Let $f, g \in L_2^+(\Omega)$. Then*

$$0 \leq M(f, g) \leq 1, \quad |S(f, g)| \leq 1.$$

Proof. By the definition of M , the condition on is equivalent to show that $0 \leq 2\mu_f\mu_g + c_1 \leq \mu_f^2 + \mu_g^2 + c_1$, which is trivially true since $\mu_f, \mu_g, c_1 \geq 0$ (for the lower bound), and $(\mu_f - \mu_g)^2 \geq 0$ (for the upper bound).

The result for S is equivalent by definition to prove that $|2\sigma_{fg} + c_2| \leq \sigma_{ff} + \sigma_{gg} + c_2$, and since $|2\sigma_{fg} + c_2| \leq 2|\sigma_{fg}| + c_2$ it is sufficient to prove that $2|\sigma_{fg}| + c_2 \leq \sigma_{ff} + \sigma_{gg} + c_2$, or equivalently that $0 \leq \sigma_{ff} + \sigma_{gg} - 2|\sigma_{fg}|$. From the definition (2) of σ_{fg} and the Cauchy-Schwartz inequality we have

$$|\sigma_{fg}| = \left| \left\langle f - \mu_f, g - \mu_g \right\rangle_{L_2} \right| \leq \left\| f - \mu_f \right\|_{L_2} \left\| g - \mu_g \right\|_{L_2},$$

and thus, again by definition of σ_f, σ_g , we obtain

$$\begin{aligned}\sigma_{ff} + \sigma_{gg} - 2|\sigma_{fg}| & \\ & \geq \left\| f - \mu_f \right\|_{L_2}^2 + \left\| g - \mu_g \right\|_{L_2}^2 - 2 \left\| f - \mu_f \right\|_{L_2} \left\| g - \mu_g \right\|_{L_2} \\ & = \left(\left\| f - \mu_f \right\|_{L_2} - \left\| g - \mu_g \right\|_{L_2} \right)^2 \geq 0,\end{aligned}$$

which concludes the proof. \square

These lemmas allows us to derive the following key estimate. The result shows that the approximation error between two functions f and g , as measured by the cSSIM, can be controlled by the squared L_2 distance of the two functions.

Proposition 5. *Let $f \in L_2^+(\Omega)$ and $c_1, c_2 > 0$. Then it holds*

$$\begin{aligned}|1 - \text{cSSIM}(f, g)| &\leq c_{fg} \|f - g\|_{L_2}^2 \\ &\leq c_f \|f - g\|_{L_2}^2 \quad \text{for all } g \in L_2^+(\Omega),\end{aligned}$$

where

$$\begin{aligned}c_{fg} &:= \frac{4}{\sigma_{ff} + \sigma_{gg} + c_2} + \frac{1}{\mu_f^2 + \mu_g^2 + c_1}, \quad (6) \\ c_f &:= \frac{4}{\sigma_{ff} + c_2} + \frac{1}{\mu_f^2 + c_1} \leq \frac{4c_1 + c_2}{c_1c_2}.\end{aligned}$$

Proof. Since $\text{cSSIM}(f, g) = M(f, g) \cdot S(f, g)$ by (3), and since $|S(f, g)| \leq 1$ by Lemma 4, it follows that

$$\begin{aligned}|1 - \text{cSSIM}(f, g)| & \\ &= |1 - S(f, g) + S(f, g) - M(f, g)S(f, g)| \\ &\leq |1 - S(f, g)| + |S(f, g)| |1 - M(f, g)| \\ &\leq |1 - S(f, g)| + |1 - M(f, g)|.\end{aligned}$$

Lemma 3 thus gives

$$\begin{aligned}|1 - \text{cSSIM}(f, g)| &\leq \quad (7) \\ &\leq \frac{\left\| (f - \mu_f) - (g - \mu_g) \right\|_{L_2}^2}{\sigma_{ff} + \sigma_{gg} + c_2} + \frac{\|f - g\|_{L_1}^2}{\mu_f^2 + \mu_g^2 + c_1}.\end{aligned}$$

Now, since the measure is normalized, it holds $\|c\|_{L_2} = |c|$ for any constant function c , and by the Hölder inequality we have $\|f\|_{L_1} \leq \|f\|_{L_2}$. Moreover, $|\mu_f - \mu_g| = \|f - g\|_{L_1}$ since both functions are non-negative. It follows that

$$\begin{aligned}\left\| (f - \mu_f) - (g - \mu_g) \right\|_{L_2} &\leq \|f - g\|_{L_2} + \left\| \mu_f - \mu_g \right\|_{L_2} \\ &= \|f - g\|_{L_2} + \left| \mu_f - \mu_g \right| \\ &\leq \|f - g\|_{L_2} + \|f - g\|_{L_1} \\ &\leq 2\|f - g\|_{L_2}.\end{aligned}$$

Combining this bound with (7), and bounding again the L_1 norm with the L_2 norm in the second term,

gives

$$\begin{aligned} |1 - \text{cSSIM}(f, g)| &\leq \frac{4 \|f - g\|_{L_2}^2}{\sigma_{ff} + \sigma_{gg} + c_2} + \frac{\|f - g\|_{L_2}^2}{\mu_f^2 + \mu_g^2 + c_1} \\ &= c_{fg} \|f - g\|_{L_2}^2 \end{aligned}$$

where $c_{fg} := 4/(\sigma_{ff} + \sigma_{gg} + c_2) + 1/(\mu_f^2 + \mu_g^2 + c_1)$. Finally

$$c_{fg} \leq \frac{4}{\sigma_{ff} + c_2} + \frac{1}{\mu_f^2 + c_1} =: c_f,$$

and since $\mu_f, \sigma_{ff} \geq 0$ we have $c_f \leq 4/c_2 + 1/c_1$, and the proof is done. \square

3.1 Conditions for equivalence

At this point one may ask if an inverse inequality holds too, proving that the two error measures are equivalent up to appropriate scaling factors. In this section we prove that this is indeed the case, but only under additional assumptions.

First, we simplify the computation of the cSSIM between functions of equal mean.

Lemma 6. *Let $f, g \in L_2^+(\Omega)$ and assume that $\mu_f = \mu_g$. Then*

$$|1 - \text{cSSIM}(f, g)| = \frac{1}{\sigma_{ff} + \sigma_{gg} + c_2} \|f - g\|_{L_2}^2.$$

Proof. Since $\mu_f = \mu_g$ by assumption, we have

$$M(f, g) = \frac{2\mu_f\mu_g + c_1}{\mu_f^2 + \mu_g^2 + c_1} = 1,$$

and thus $\text{cSSIM}(f, g) = S(f, g)$. In this case (5) gives

$$\begin{aligned} |1 - \text{cSSIM}(f, g)| &= |1 - S(f, g)| \\ &= \frac{\|(f - \mu_f) - (g - \mu_g)\|_{L_2}^2}{\sigma_{ff} + \sigma_{gg} + c_2} \\ &= \frac{\|f - g\|_{L_2}^2}{\sigma_{ff} + \sigma_{gg} + c_2}, \end{aligned}$$

which is the equality in the statement. \square

Using this lemma we can formulate the claimed equivalence, which holds for the function class

$$\mathcal{F}(R_1, R_2) := \left\{ f \in L_2^+(\Omega) : \|f\|_{L_2} \leq R_2, \|f\|_{L_1} = R_1 \right\},$$

where $m, R \geq 0$ are given parameters.

Proposition 7. *For each $R_1, R_2 \geq 0$ and $f, g \in \mathcal{F}(R_1, R_2)$ it holds*

$$\frac{1}{4R_2^2 + c_2} \|f - g\|_{L_2}^2 \leq |1 - \text{cSSIM}(f, g)| \leq \frac{1}{c_2} \|f - g\|_{L_2}^2.$$

Proof. Since $f, g \in \mathcal{F}(R_1, R_2)$ for some $R_1, R_2 \geq 0$ we have $\mu_f = \mu_g = R_1$, and thus we can use Lemma 6 and just find lower and upper bounds for the constant $\sigma_{ff} + \sigma_{gg} + c_2$.

The lower bound is simply given by $\sigma_{ff} + \sigma_{gg} + c_2 \geq c_2$, since $\sigma_{ff}, \sigma_{gg} \geq 0$. For the upper bound we have by (2) that

$$\begin{aligned} \sigma_{ff} &= \|f - \mu_f\|_{L_2(\Omega)}^2 \leq \|f\|_{L_2(\Omega)}^2 + \|\mu_f\|_{L_2(\Omega)}^2 \\ &= \|f\|_{L_2(\Omega)}^2 + \mu_f^2 = \|f\|_{L_2(\Omega)}^2 + \|f\|_{L_1(\Omega)}^2 \\ &\leq 2\|f\|_{L_2(\Omega)}^2 \leq 2R_2^2, \end{aligned}$$

and similarly for σ_{gg} . It follows that $\sigma_{ff} + \sigma_{gg} + c_2 \leq 4R_2^2 + c_2$, which is the desired upper bound. \square

This proposition proves that under certain conditions the cSSIM is equivalent to the L_2 norm, and this in particular implies that the rates of Proposition 5 (i.e., the exponent 2) can not be improved if they have to hold for general $f, g \in L_2^+(\Omega)$.

Moreover, since ν is normalized it holds $\|f\|_{L_2(\Omega)} \leq \|f\|_{L_\infty(\Omega)}$, and thus for f, g that represent reasonable images it is easy to find $R_2 > 0$ such that $\|f\|_{L_2(\Omega)}, \|g\|_{L_2(\Omega)} \leq R_2$. On the other hand, the condition $\mu_f = \mu_g$ is not automatically verified for arbitrary pairs of functions f, g . Nevertheless, if a function $f \in L_2^+(\Omega)$ is approximated in the L_2 sense by a sequence $\{f_n\} \subset L_2^+(\Omega)$, since as observed before it holds

$$|\mu_f - \mu_{f_n}| \leq \|f - f_n\|_{L_1(\Omega)} \leq \|f - f_n\|_{L_2(\Omega)}$$

we have $\mu_{f_n} \rightarrow \mu_f$. In this sense, we should expect to see an equivalence in the spirit of Proposition 7 when the two error measures are used on L_2 converging approximations. We will verify this intuition in the numerical experiments.

In general we can not expect an equivalence like the one of Proposition 7 to hold in general, since for all $f, g \in L_2^+(\Omega)$ it holds $|1 - \text{cSSIM}(f, g)| \leq 2$ by Lemma 4, but on the other hand there exists $f, g \in L_2^+(\Omega)$ that have unboundedly large L_2 distance. This situation is ruled out in Proposition 7 by the bound on the L_2 norm of functions in \mathcal{F} , and it would be interesting to investigate if this condition is also necessary, or if the equal-mean condition is also required to have equivalence. Namely, is it possible to construct sequences $\{f_n\}, \{g_n\}$ in the unit ball of $L_2^+(\Omega)$, such that for all $c > 0$ there exists $\bar{n} \in \mathbb{N}$ with $c \|f_n - g_n\|_{L_2} > |1 - \text{cSSIM}(f_n, g_n)|$ for all $n \geq \bar{n}$?

4 Rates of convergence of the cSSIM for concrete image interpolation methods

In the following, we exploit the theoretical findings presented in Section 3 and we provide some convergence results in terms of the cSSIM for commonly used image interpolation methods. First, we consider for the case of gridded data the bilinear interpolation method and the Hermite bicubic interpolation method. Then, we consider the framework of kernel-based interpolation, which is particularly suitable for scattered data.

We consider for simplicity $\Omega = [a, b] \times [c, d] \subset \mathbb{R}^2$. We are interested in obtaining bounds on the convergence of these interpolation methods with respect to the cSSIM from known results on their L_2 convergence. The latter results are usually formulated in terms of the smoothness of the target function f , and to this end we will assume in the following that f is an element of the Sobolev space $W_2^\tau(\Omega)$ of suitable fractional or integer order $\tau > 0$ (see e.g. Chapter 3 in [16]).

Moreover, we denote as $C^{k,l}(\Omega)$ the set of func-

tions whose derivatives $\partial^{i+j} f / (\partial x^i \partial y^j)$ are continuous on Ω for $0 \leq i \leq k$ and $0 \leq j \leq l$.

The rate of approximation of the various methods are quantified in terms of the density and distribution of the interpolation points $X \subset \Omega$, that is quantified by means of the fill distance

$$h_{X,\Omega} := \sup_{y \in \Omega} \min_{x \in X} \|x - y\|, \quad (8)$$

which is a generalization of the grid size that is suitable also for scattered meshes.

4.1 Bilinear interpolation

Let $f \in C^{0,0}(\Omega)$, $f \in W_2^2(\Omega)$, and let $E_{m,n}$ be a $m \times n$ equispaced grid of interpolation nodes in Ω with equal horizontal and vertical spacing $s > 0$. Consequently, the fill distance is $h_{E_{m,n},\Omega} := \sqrt{2}s/2$ and it represents in this case the pixel size. The unique bilinear interpolant f_b of f at $E_{m,n}$ is constructed upon 2×2 local neighborhoods. More precisely, letting $z_{11} = (x_1, y_1)$, $z_{21} = (x_2, y_1)$, $z_{12} = (x_1, y_2)$, $z_{22} = (x_2, y_2) \in E_{m,n}$ be the neighborhood nodes related to an evaluation point $\xi = (\xi_1, \xi_2) \in \Omega$, that is ξ is contained in the rectangle defined by the vertices $z_{11}, z_{21}, z_{12}, z_{22}$, we have

$$f_b(\xi_1, \xi_2) = c_0 + c_1 \xi_1 + c_2 \xi_2 + c_3 \xi_1 \xi_2,$$

where the coefficients c_0, \dots, c_3 are determined by solving the linear system

$$\begin{bmatrix} 1 & x_1 & y_1 & x_1 y_1 \\ 1 & x_1 & y_2 & x_1 y_2 \\ 1 & x_2 & y_1 & x_2 y_1 \\ 1 & x_2 & y_2 & x_2 y_2 \end{bmatrix} \begin{bmatrix} c_0 \\ c_1 \\ c_2 \\ c_3 \end{bmatrix} = \begin{bmatrix} f(z_{11}) \\ f(z_{21}) \\ f(z_{12}) \\ f(z_{22}) \end{bmatrix}. \quad (9)$$

The L_2 -error between f and f_b on Ω can be bounded as (see e.g. [10])

$$\|f - f_b\|_{L_2} \leq Ch \|f\|_{W_2^\tau},$$

where $C > 0$ is a constant independent of h . Therefore, from Proposition 5 we get

$$|1 - \text{cSSIM}(f, f_b)| \leq c_f C^2 h^2 \|f\|_{W_2^\tau}^2.$$

4.2 Hermite bicubic interpolation

Differently with respect to the bilinear interpolation case, the Hermite bicubic interpolant f_c is built upon 4×4 neighborhoods. In addition to the constraints imposed by the function values $f(z_{11}), f(z_{21}), f(z_{12}), f(z_{22})$, the function f_c also interpolates $\partial f / (\partial x)$, $\partial f / (\partial y)$ and $\partial^2 f / (\partial x \partial y)$ at $z_{11}, z_{21}, z_{12}, z_{22}$. The extremal nodes of the neighborhood are indeed exploited in order to estimate such derivatives at the 2×2 internal nodes.

Therefore, the interpolant f_c evaluated at ξ takes the form

$$f_c(\xi_1, \xi_2) = \sum_{0 \leq i, j \leq 3} c_{ij} \frac{\partial^{i+j} f}{\partial x^i \partial y^j}(\xi_1, \xi_2),$$

where the coefficients c_{ij} are determined by solving the linear system related to the interpolation task, similarly to (9).

For $f \in C^{1,1}(\Omega) \cap W_2^4(\Omega)$, the paper [2] gives the bound

$$\|f - f_c\|_{L_2} \leq Ch^3 \|f\|_{W_2^4},$$

and thus by virtue of Proposition 5 we obtain

$$|1 - \text{cSSIM}(f, f_c)| \leq c_f C^2 h^6 \|f\|_{W_2^4}^2.$$

4.3 Kernel-based interpolation

Let $K : \Omega \times \Omega \rightarrow \mathbb{R}$ be a strictly positive definite kernel, i.e., for any set $X \subset \Omega$ of pairwise distinct points the kernel matrix $K = (K_{ij}) = K(x_i, x_j)$, $x_i, x_j \in X$ is positive definite.

The kernel interpolant f_k of $f \in C(\Omega)$ at n pairwise distinct points $X \subset \Omega$ is defined as

$$f_k(\xi_1, \xi_2) = \sum_{i=1}^n \alpha_i K(\xi, x_i), \quad x_i \in X, \xi \in \Omega,$$

with coefficients $\alpha = (\alpha_1, \dots, \alpha_n)^\top \in \mathbb{R}^n$ that solve the linear system

$$K\alpha = f,$$

where K is the kernel matrix on X and $f = (f(x_1), \dots, f(x_n))^\top$.

It is known that if the kernel is additionally translational invariant, i.e., $K(x, y) := \Phi(x - y)$ for some

$\Phi : \mathbb{R}^d \rightarrow \mathbb{R}$, then under certain assumptions one can show that there exists $\tau > d/2$ such that for each $f \in W_2^\tau(\Omega)$ it holds

$$\|f - f_k\|_{L_2} \leq Ch^\tau \|f\|_{W_2^\tau},$$

with a constant $C > 0$ independent of f . We remark that the precise value of τ is given by the rate of polynomial decay of the Fourier transform of Φ , and this value is connected to the smoothness of K . We do not give further explanations here, and we refer to [23] for a detailed discussion.

In this setting Proposition 5 gives that for each $f \in L_2^+(\Omega) \cap W_2^\tau(\Omega)$ it holds

$$|1 - \text{cSSIM}(f, f_k)| \leq c_f C^2 h^{2\tau} \|f\|_{W_2^\tau}^2. \quad (10)$$

As notable examples, we report in particular the error bounds related to the two kernels considered in [15]. We remark that these new bounds are strict improvements over the results proven in that paper.

- If K is a (d, k) -Wendland kernel with $d = 2$ and $k = 1$, i.e., $\Phi(x) = \varphi_1(\|x\|)$ with $\varphi_1(r) = (1 - r)_+^4 (4r + 1)$, then $\tau = d/2 + k + 1/2 = 1 + 1 + 1/2 = 5/2$ (see [23]), and thus (10) gives

$$|1 - \text{cSSIM}(f, f_k)| \leq c_f C^2 h^5 \|f\|_{W_2^{5/2}}^2.$$

- If K is a cubic Matérn kernel, i.e., $\Phi(x) = \varphi_2(\|x\|)$ with $\varphi_2(r) = e^{-r}(15 + 15r + 6r^2 + r^3)$, then $\tau = (d + 7)/2 = 9/2$ (see [23]), and thus (10) gives

$$|1 - \text{cSSIM}(f, f_k)| \leq c_f C^2 h^9 \|f\|_{W_2^{9/2}}^2.$$

Finally, we recall that it is common in practice to solve a regularized interpolation problem with kernel matrix $(K + \lambda I)$ with $\lambda > 0$ in order to improve the numerical conditioning of the system. Results are known to select λ small enough such that the same convergence rates as in (10) are obtained (see [24]).

5 Numerical tests

The experiments are carried out in PYTHON 3.6. The code to replicate the experiments is publicly available¹.

To verify the convergence estimates discussed in Section 4, we perform numerical tests taking the same examples studied in [15], i.e. the functions $f_1, f_2 : \Omega \rightarrow \mathbb{R}, \Omega = [-1, 1]^2$, defined as

$$\begin{aligned} f_1(x) &= 2(x_1 x_2)^2 - \text{sinc}(x_1) \text{sinc}(x_2) + 1, \\ f_2(x) &= e^{-(x_1+x_2)} - 3x_1 + x_2 + 5. \end{aligned}$$

As interpolation sets, we take equispaced gridded data $X_i \subset \Omega, i = 1, \dots, 4$, whose step is $s_i = 2^{-i+2}/5$. The reconstructions are then evaluated on a finer grid with step $5 \cdot 10^{-3}$. Moreover, to approximate the cSSIM, we compute the SSIM on the evaluation grid and we express the results in terms of the dissimilarity $\text{DSSIM} := 1 - \text{SSIM}$.

We report the results obtained by performing bilinear and bicubic interpolation in Figure 1, while in Figure 2 we display the results achieved by kernel-based interpolation. More precisely, varying the interpolation set $X_i, i = 1, \dots, 4$, we display the DSSIM (blue dots), the corresponding regression line (dashed orange), the bound obtained in Proposition 5 with c_f (dashed green) and by considering the factor c_{fg} defined in the proof (dashed red). We point out that in these experiments we use an own implementation of the interpolation methods, and in particular we use the exact values of the partial derivatives of the functions in the case of Hermite bicubic interpolation, in order to verify the investigated theoretical bounds.

6 Image interpolation experiments

In the following tests, the image interpolation processes are performed by means of the bilinear and bicubic implementation of the OpenCV Python library [3].

¹https://github.com/GabrieleSantin/cssim_convergence.

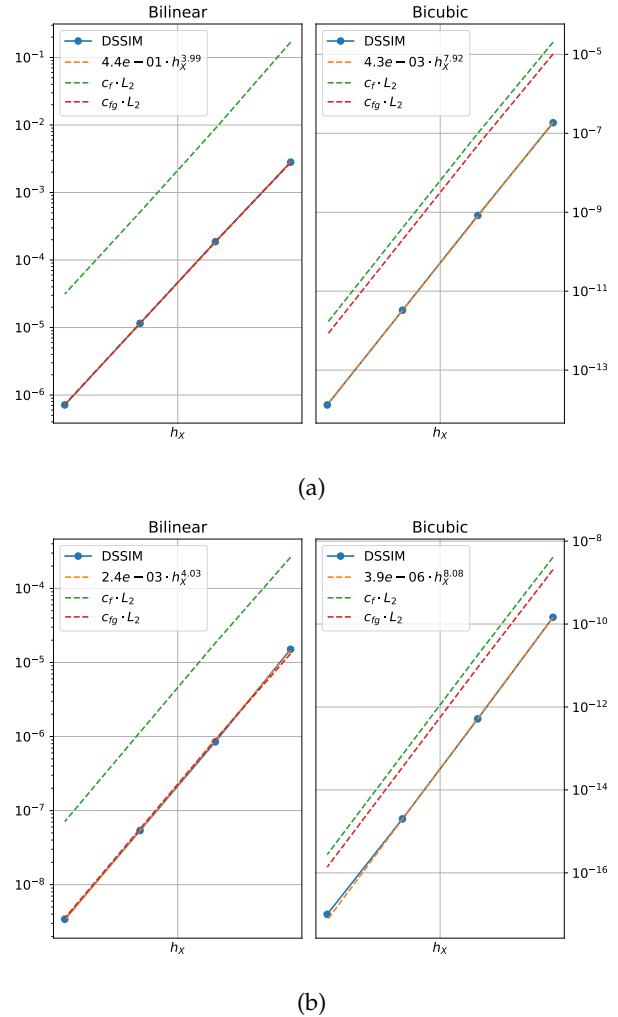
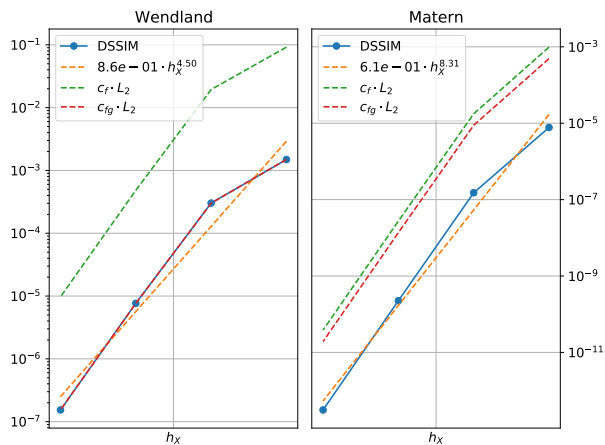
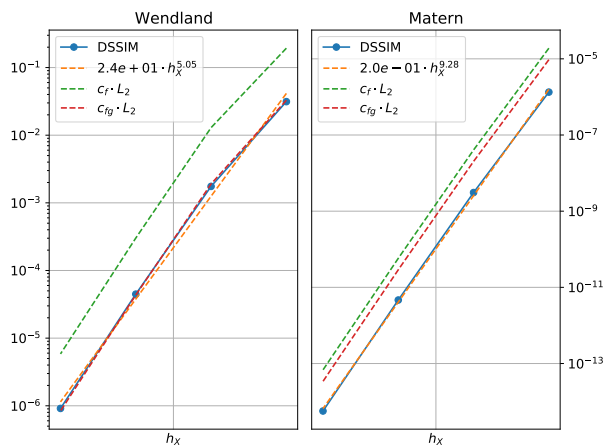


Figure 1: Decay of the DSSIM index for bilinear and bicubic interpolation, with target function f_1 (panel (1a)) and f_2 (panel (1b)).



(a)



(b)

Figure 2: Decay of the DSSIM index for the two kernels φ_1 , φ_2 , with target function f_1 (panel (2a)) and f_2 (panel (2b)).

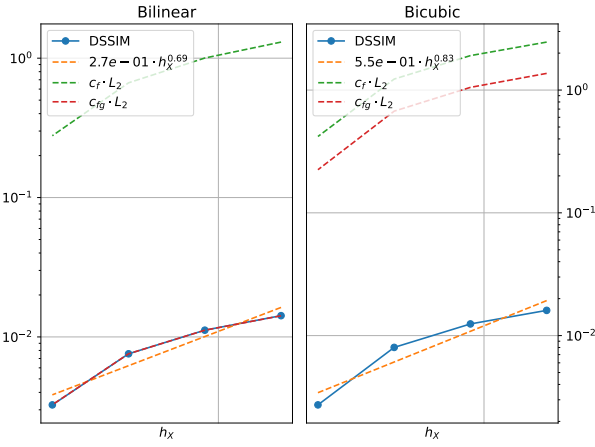


Figure 3: Top left: *baboon*. Top right: *peppers*. Bottom left: *cameraman*. Bottom right: *Lenna*.

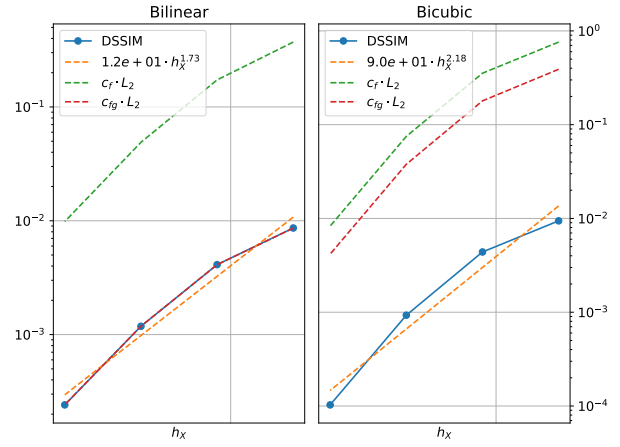
We consider four 512×512 images, displayed in Figure 3 and whose values are normalized between $[0, 1]$, which are well-known in the context of image processing. Each image is then undersampled to be 40×40 , 80×80 , 160×160 , 320×320 . The resized images are then interpolated in order to recover a 512×512 matrix, and the reconstruction is compared to the original image. We point out that the step of interpolation dataset is defined to be the reciprocal of the number of pixels for each dimension.

7 Discussion and conclusions

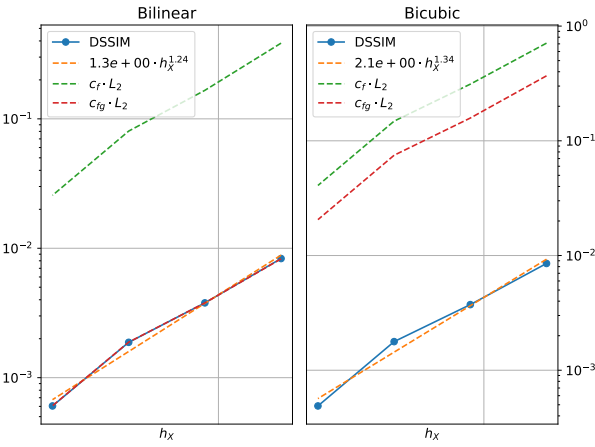
In this paper we considered the continuous SSIM introduced in [15], and we shed some light on its relation with the classical SSIM and with the L_2 norm. In particular, we deepened the relationship between cSSIM and L_2 norm by providing both upper and lower bounds for the cSSIM (Section 3), and we used those bounds to present a detailed analysis of the cSSIM-convergence rates of some well-known im-



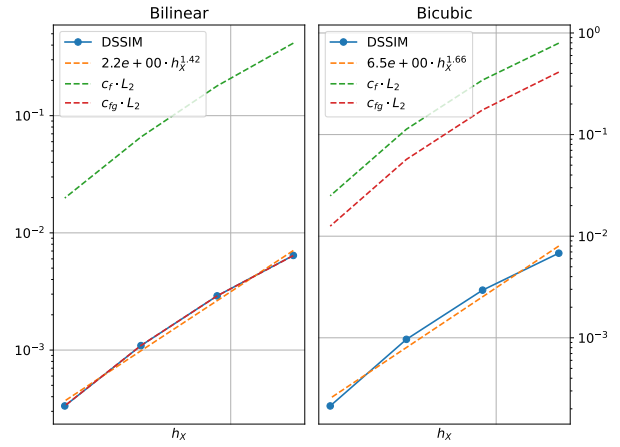
(a)



(a)



(b)



(b)

Figure 4: Decay of the DSSIM index for *baboon* (panel (4a)) and *peppers* (panel (4b)).

Figure 5: Decay of the DSSIM index for *cameraman* (panel (5a)) and *Lenna* (panel (5b)).

age interpolation methods. To our knowledge, these are the first explicit results on convergence rates of image interpolation methods in terms of the SSIM.

The numerical tests carried out in Section 5 confirm the theoretical findings of Section 4, as well as the statement of Proposition 5. In particular, in Figure 1 we observe a *superconvergence* phenomenon concerning bilinear and bicubic interpolation, which we argue to be due to the regularity of the test functions.

In Section 6 we carried out some image interpolation tests considering different standard test pictures. Here, the rates of convergence are slowed down by the irregularity of the functions which underlie the images. Moreover, in this case the partial derivatives employed in the Hermite bicubic interpolation are not exact. Indeed, they are estimated by the implementation of OpenCV by taking 4×4 neighborhoods in the images (see Section 4.2).

We observe that the convergence rates related to *baboon* and *peppers*, as depicted in Figure 4, are slower than the ones corresponding to *Lenna* and *cameraman*, which are displayed in Figure 5. This is probably due the presence of more complex structures and more frequent gray-value variations in the former couple of pictures. These rates are nevertheless perfectly aligned with the decay rates of the L_2 error, as predicted by our theory.

These theoretical results and experimental findings prove that one may infer significant information on the behavior of the SSIM by looking at the much more classical L_2 error, which is a convex, thoroughly studied, and easy to implement measure.

Future work will be devoted to the investigation of the insight that complex structures may lead to different rates of approximation. Exploiting such structures in the images may lead to further and more accurate theoretical bounds in terms of the cSSIM.

Moreover, the SSIM have been used as a loss function in supervised learning to enforce a perceptually accurate reconstruction of images. In this setting, some approaches have been adopted to overcome the fact that the SSIM (as well as the cSSIM) induces a non convex loss [5]. In view of our the-

oretical results, it seems interesting to investigate if the minimization of the L_2 loss may provide a reliable surrogate of the SSIM loss.

Acknowledgments

The authors acknowledge their membership in the “Research Italian Network on Approximation (RITA)”, in the GNCS-IN δ AM and in the group “Teoria dell’Approssimazione e Applicazioni (TAA)” of the Unione Matematica Italiana (UMI). FM is supported by the financial contribution from the agreement ASI-INAF n.2018-16-HH.0.

References

- [1] M. Al-nasrawi, G. Deng, and B. Thai. Edge-aware smoothing through adaptive interpolation. *Signal Image Video Process.*, 12(2):347–354, 2018.
- [2] B. Bialecki and X.-C. Cai. H1-norm error bounds for piecewise hermite bicubic orthogonal spline collocation schemes for elliptic boundary value problems. *SIAM J. Numer. Anal.*, 31(4):1128–1146, Aug. 1994.
- [3] G. Bradski. The OpenCV Library. *Dr. Dobb’s Journal of Software Tools*, 2000.
- [4] D. Brunet, J. Vass, E. R. Vrscay, and Z. Wang. Geodesics of the structural similarity index. *Appl. Math. Lett.*, 25(11):1921–1925, 2012.
- [5] D. Brunet, E. R. Vrscay, and Z. Wang. On the mathematical properties of the structural similarity index. *IEEE Trans. Image Process.*, 21(4):1488–1499, 2012.
- [6] Y. Chen, Z. X. Lyu, X. Kang, and Z. J. Wang. A rotation-invariant convolutional neural network for image enhancement forensics. In *2018 IEEE International Conference on Acoustics, Speech and Signal Processing (ICASSP)*, pages 2111–2115, 2018.

- [7] S. De Marchi, W. Erb, and F. Marchetti. Spectral filtering for the reduction of the Gibbs phenomenon for polynomial approximation methods on Lissajous curves with applications in MPI. *Dolomites Res. Notes on Approx.*, 10:128–137, 2017.
- [8] S. De Marchi, W. Erb, F. Marchetti, E. Perracchione, and M. Rossini. Shape-driven interpolation with discontinuous kernels: Error analysis, edge extraction, and applications in magnetic particle imaging. *SIAM J. Sci. Comput.*, 42(2):B472–B491, 2020.
- [9] S. De Marchi, F. Marchetti, and E. Perracchione. Jumping with variably scaled discontinuous kernels (VSDKs). *BIT Numer. Math.*, 60:441–463, 2020.
- [10] P. Getreuer. Linear methods for image interpolation. *Image Process. Line*, 1, 2011.
- [11] H. Huang, R. He, Z. Sun, and T. Tan. Wavelet-srnet: A wavelet-based CNN for multi-scale face super resolution. In *IEEE International Conference on Computer Vision, ICCV 2017, Venice, Italy, October 22-29, 2017*, pages 1698–1706. IEEE Computer Society, 2017.
- [12] N. Jiang and L. Wang. Quantum image scaling using nearest neighbor interpolation. *Quantum Inf. Process.*, 14(5):1559–1571, 2015.
- [13] Jung Woo Hwang and Hwang Soo Lee. Adaptive image interpolation based on local gradient features. *IEEE Signal Processing Letters*, 11(3):359–362, 2004.
- [14] S. Khan, D. Lee, M. A. Khan, A. R. Gilal, and G. Mujtaba. Efficient edge-based image interpolation method using neighboring slope information. *IEEE Access*, 7:133539–133548, 2019.
- [15] F. Marchetti. Convergence rate in terms of the continuous SSIM (cSSIM) index in RBF interpolation. *Dolomites Res. Notes on Approx.*, 14(1), 2021.
- [16] W. McLean. *Strongly elliptic systems and boundary integral equations*. Cambridge university press, 2000.
- [17] A. Rehman, K. Zeng, and Z. Wang. Display device-adapted video quality-of-experience assessment. In B. E. Rogowitz, T. N. Pappas, and H. de Ridder, editors, *Human Vision and Electronic Imaging XX, San Francisco, California, USA, February 9-12, 2015*, volume 9394 of *SPIE Proceedings*, page 939406. SPIE, 2015.
- [18] O. Rukundo and B. T. Maharaj. Optimization of image interpolation based on nearest neighbour algorithm. In *2014 International Conference on Computer Vision Theory and Applications (VIS-APP)*, volume 1, pages 641–647, 2014.
- [19] M. P. Sampat, Z. Wang, S. Gupta, A. C. Bovik, and M. K. Markey. Complex wavelet structural similarity: A new image similarity index. *IEEE Trans. Image Process.*, 18(11):2385–2401, 2009.
- [20] W. Siu and K. Hung. Review of image interpolation and super-resolution. In *Proceedings of The 2012 Asia Pacific Signal and Information Processing Association Annual Summit and Conference*, pages 1–10, 2012.
- [21] P. Smith. Bilinear interpolation of digital images. *Ultramicroscopy*, 6(2):201–204, 1981.
- [22] Z. Wang, A. C. Bovik, H. R. Sheikh, and E. P. Simoncelli. Image quality assessment: from error visibility to structural similarity. *IEEE Trans. Image Process.*, 13(4):600–612, 2004.
- [23] H. Wendland. *Scattered Data Approximation*, volume 17 of *Cambridge Monographs on Applied and Computational Mathematics*. Cambridge University Press, Cambridge, 2005.
- [24] H. Wendland and C. Rieger. Approximate interpolation with applications to selecting smoothing parameters. *Numerische Mathematik*, 101(4):729–748, 2005.
- [25] J. Yamanaka, S. Kuwashima, and T. Kurita. Fast and accurate image super resolution by deep

CNN with skip connection and network in network. In D. Liu, S. Xie, Y. Li, D. Zhao, and E. M. El-Alfy, editors, *Neural Information Processing - 24th International Conference, ICONIP 2017, Guangzhou, China, November 14-18, 2017, Proceedings, Part II*, volume 10635 of *Lecture Notes in Computer Science*, pages 217–225. Springer, 2017.

- [26] K. Zeng, S. Ding, and W. Jia. Single image super-resolution using a polymorphic parallel CNN. *Appl. Intell.*, 49(1):292–300, 2019.